FIGURE 4-42 The TO-18 packaged capacitors.

For a more easy and rapid identification of the sets of capacitors in the first capacitors shipped to us by Radiant a colored paint has been applied to the upper face of the metal cap following the designations in Table 4-6. Moreover information about the area size of the oxide masks and platinum for both the two driving electrodes are also given in Table 4-6. Radiant states a little fatigue or imprint for these capacitors below 85° [165]. The capacitors have been recovered prior to shipment to eliminate process damage so there should be no need to execute recoveries in the future. Anyway, if necessary, recovering of a capacitor can be made executing a 9V square wave at 1Hz for 100s at room temperature.

TABLE 4-6 Summary of sizes of the oxide masks and platinum areas of the two driving electrodes and color of the paint applied to the metal cap for the identification of the capacitor.

DIE Designation	Cap Color	Large Platinum (μ^2)	Large Oxide Mask (μ^2)	Small Platinum (μ^2)	Small Oxide Mask (μ^2)
135-100-25	WHITE	133,750	145,800	10,000	10,404
235-150-50	RED	465,850	484,700	22,500	23,104
275-50-10	BLUE	347,150	363,000	2,500	2,704
160-50-25	BLACK	145,500	156,800	2,500	2,704
135-150-100	YELLOW	233,750	253,800	22,500	23,104

5.3.2 CHARACTERIZATION IN THE P-E DOMAIN

As with the others ferroelectric capacitors discussed in previous sections investigation of these new devices has started with the characterization of the behavior in the P-E domain.

Experimental data acquisitions have been performed changing the amplitude and the frequency of the voltage applied to the driving electrodes. The Sawyer-Tower conditioning circuit above discussed has been used to convert the polarization of the ferroelectric in a proportional voltage signal.

Chosen, once again, the model (4.8) to represent the dynamic behavior of the ferroelectric capacitor a set of parameters (a, b, c, τ) which make a good fitting of the predicted hysteresis by the model over the experimental hysteresis, has been identified by the tool in section 5.1.3.

Figure 4-43 shows some examples of experimental P-E hysteresis (red line) for the capacitor C3 designated as 235-150-50 (red cap) for three amplitudes of the driving voltage ($6V_{pp}$, $10V_{pp}$ and $15V_{pp}$) and two different frequencies (1kHz and 10kHz) together with the hysteresis predicted by the model (4.8) with the identified parameters (blu dotted line).

As an example, in Table 4-7 the parameters identified for the same capacitor for different amplitudes and frequencies of the driving voltage, are reported. Furthermore, the value of the root mean square type functional J that computes (as a percentage) the residuals between the predicted (via the model) values and the observed values of the polarization, together with the values of the error defined as the root square residuals, have been included. Finally the value of the remnant polarizations evaluated by the experimental hysteresis are reported in the last right column.

The same procedure has been adopted for all the others capacitors and for the sake of brevity their related hysteresis and identified parameters will not reported here. Figure 4-44 shows the trend of the parameters a, b, c for the capacitor C3 designated as 235-150-50 (red cap) as a function of the amplitude (Figure 4-44a,c and e) and frequency (Figure 4-44b,d and f) of the driving voltage. A dependence on both the amplitude and the frequency is clearly visible.

Driving 6 V_{pp}

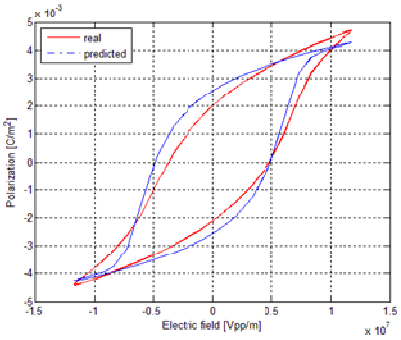

1 kHz

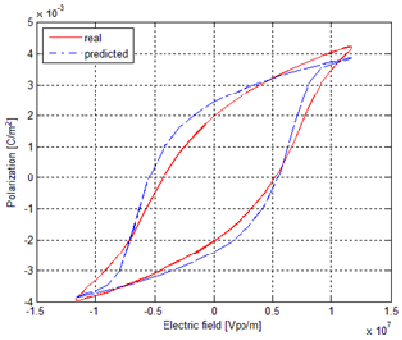

10 kHz

Driving 10 V_{pp}

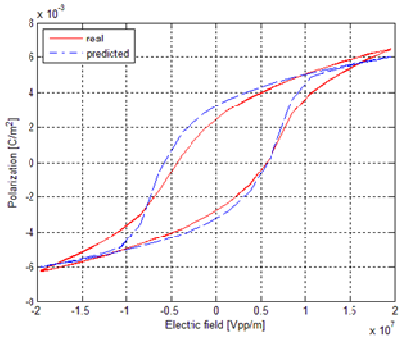

1 kHz

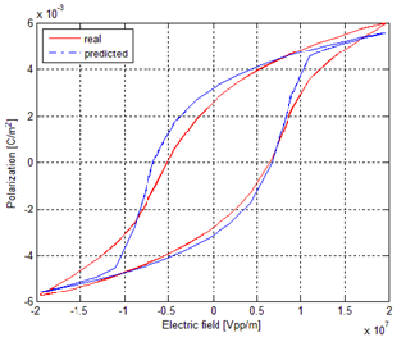

10 kHz

Driving 15 V_{pp}

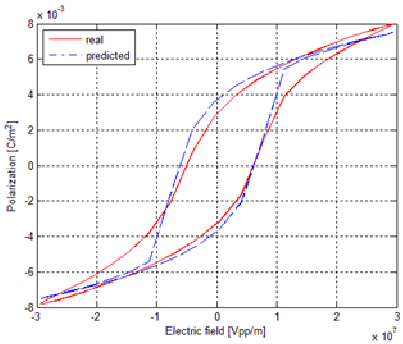

1 kHz

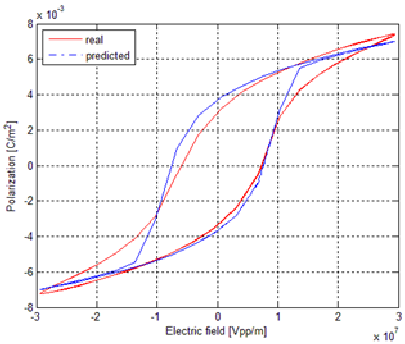

10 kHz

FIGURE 4-43 Examples of experimental P-E hysteresis (red line) for three amplitudes and two frequencies of the driving voltage together with the hysteresis predicted by the model (4.8) with the identified parameters (blu dotted line).

TABLE 4-7 The parameters identified for the capacitor C3 designated as 235-150-50 (red cap) for different amplitudes and frequencies of the driving voltage.

Parameters Identified for the capacitor C3 - 235-150-50 (red cap)

Frequency	a	b	c	τ	J	error	P_r
			Driving 20 V_{pp}				
100kHz	0.0018	125.787	1.176e-12	6.772e-10	5.870	0.003	3.80e-3
50kHz	4.513e-4	35.812	3.510e-13	6.772e-10	7.374	0.007	3.55e-3
10kHz	7.750e-5	7.568	8.502e-14	6.772e-10	7.955	0.008	3.20e-3
1kHz	6.683e-6	0.695	1.004e-14	6.772e-10	8.422	0.009	3.10e-3
500Hz	3.524e-6	0.459	7.709e-15	6.772e-10	7.782	0.008	2.77e-3
			Driving 15 V_{pp}				
100kHz	0.002	130.372	1.023e-12	6.772e-10	6.555	0.003	3.50e-3
50kHz	3.627e-4	35.420	2.979e-13	6.772e-10	7.960	0.007	3.20e-3
10kHz	7.209e-5	8.118	7.752e-14	6.772e-10	8.338	0.007	2.98e-3
1kHz	7.431e-6	0.890	1.085e-14	6.772e-10	8.571	0.008	2.89e-3
500Hz	2.530e-6	0.405	5.858e-15	6.772e-10	7.769	0.007	2.50e-3
			Driving 10 V_{pp}				
100kHz	0.001	135.062	7.693e-13	6.772e-10	8.867	0.003	2.90e-3
50kHz	2.728e-4	37.983	2.286e-13	6.772e-10	9.339	0.006	2.68e-3
10kHz	5.486e-5	8.437	5.908e-14	6.772e-10	9.418	0.006	2.55e-3
1kHz	4.768e-6	0.808	7.493e-15	6.772e-10	9.217	0.007	2.43e-3
500Hz	1.8e-6	0.420	4.515e-15	6.772e-10	9.180	0.007	2.07e-3
			Driving 6 V_{pp}				
100kHz	8.399e-4	209.971	5.527e-13	6.772e-10	12.139	0.003	2.00e-3
50kHz	1.940e-4	53.728	1.542e-13	6.772e-10	12.128	0.005	1.90e-3
10kHz	4.209e-5	10.955	3.983e-14	6.772e-10	11.589	0.005	1.96e-3
1kHz	3.872e-6	0.978	5.098e-15	6.772e-10	11.280	0.006	1.99e-3
500Hz	1.407e-6	0.470	2.916e-15	6.772e-10	10.763	0.006	1.73e-3

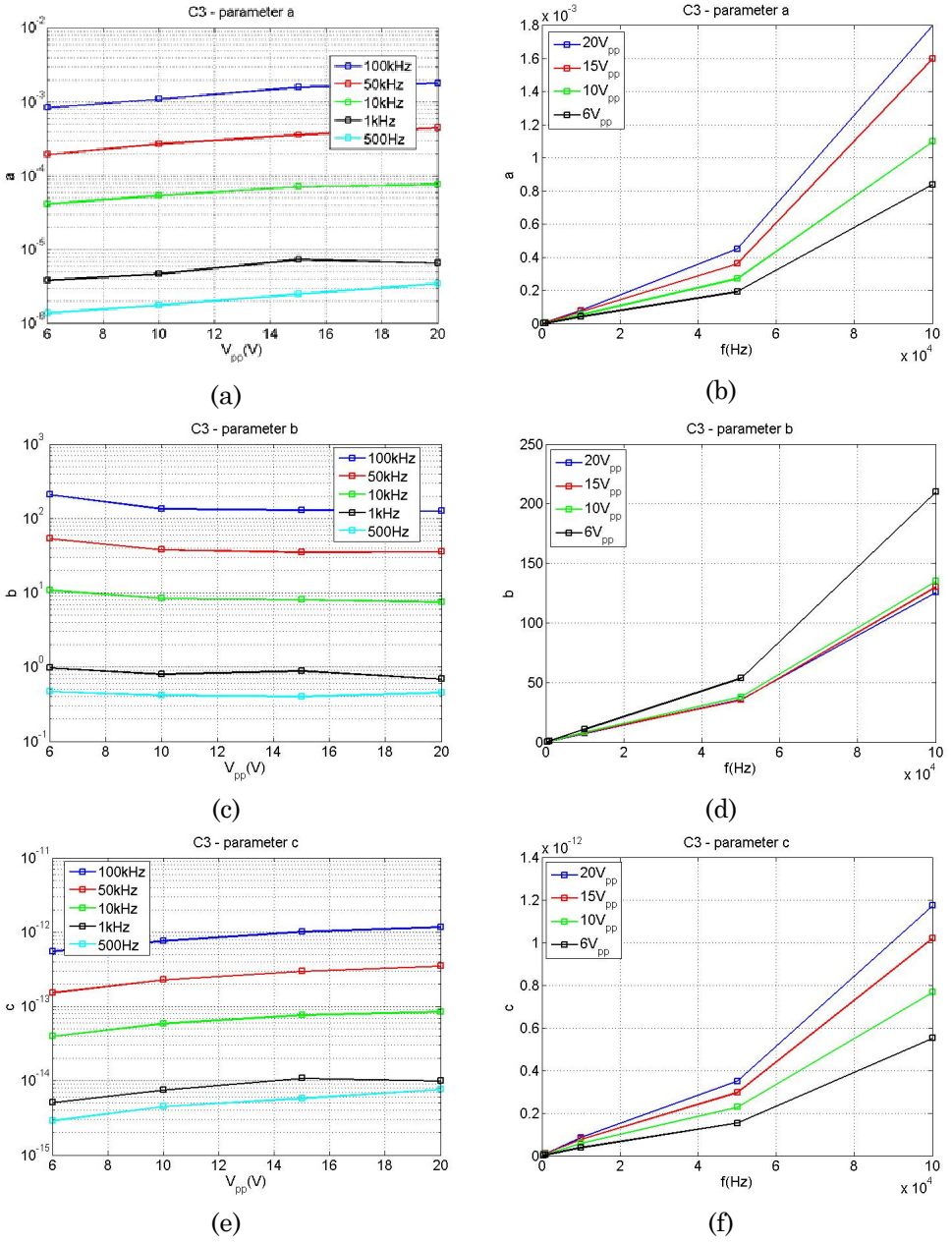

FIGURE 4-44 Trend of the parameters *a*, *b*, and *c* for the capacitor C3 designated as 235-150-50 (red cap) as a function of the amplitude ((a), (c) and (e)) and frequency ((b), (d) and (f)) of the voltage applied to the driving electrodes.

A comparison of the identified parameters for capacitors of the same type and having the same group code (a comparison between capacitors belonging to different groups will be possible when all the designed capacitors will be shipped us by Radiant) has been performed to the purpose to investigate the technology process and to verify that capacitors belonging to the same group can be stated to be equals. Figure 4-45 shows the results of the comparison for three capacitors (C2, C3, C4) designated as 235-150-50 (red cap) from the same group (i.e. having the same binary code 0001) as a function of the amplitude (Figure 4-45a, c and e) and frequency (Figure 4-45b, d and f) of the voltage applied to the driving electrodes.

In addition to the dependence of the value of the parameters on the amplitude and frequency of the applied driving voltage it is possible to observe that parameters for the three capacitors are rather equals.

This latter is a remarkable and comforting result which represents a milestone in our analysis and allows us to conclude that the three capacitors (belonging to the same group) are equals. The importance of this conclusion will be clear in next sections where the coupled configuration will be investigated.

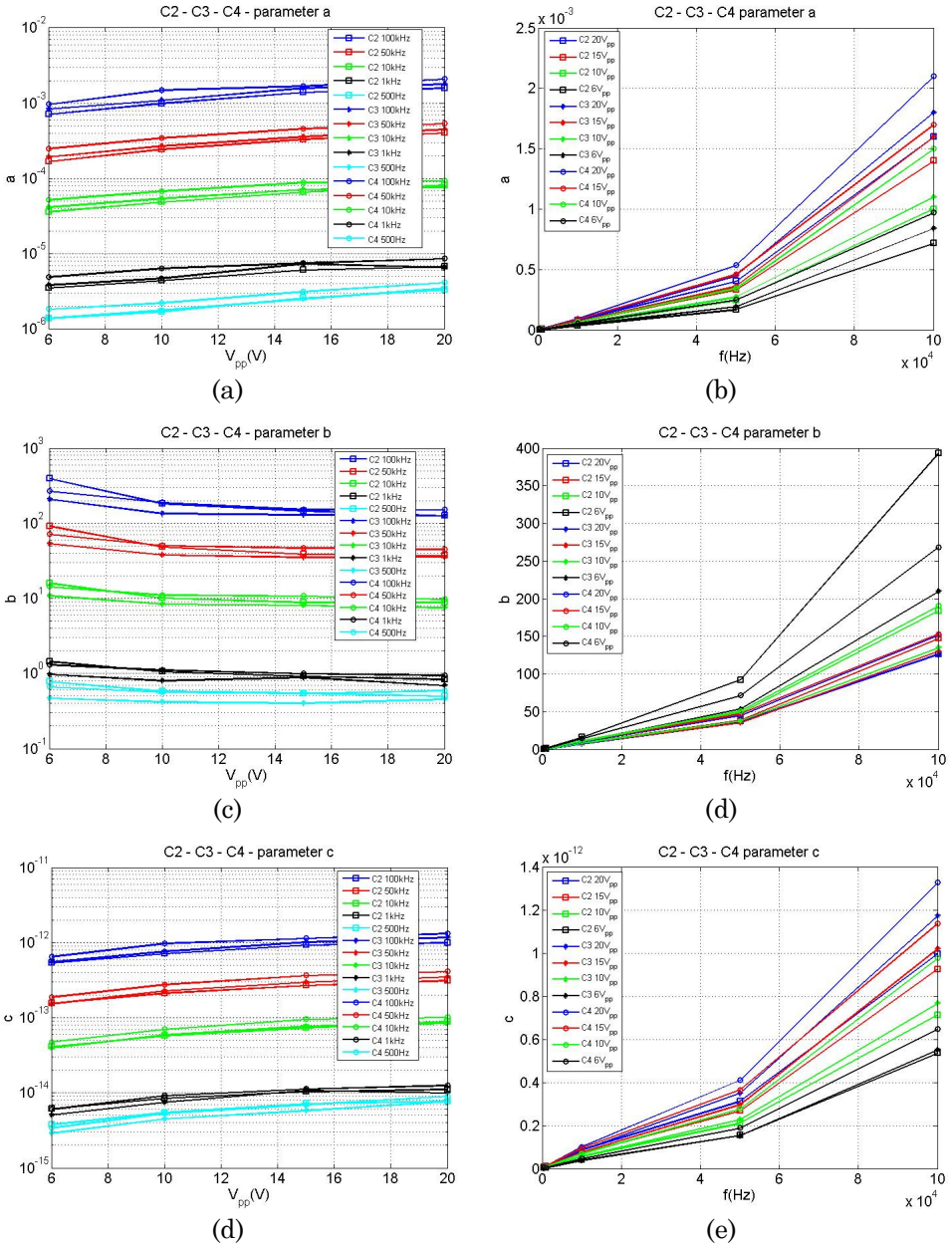

FIGURE 4-45 Comparison for three capacitors (C2, C3, C4) designated as 235-150-50 (red cap) from the same group (i.e. having the same binary code 0001) as a function of the amplitude ((a), (c) and (e)) and frequency ((b), (d) and (f)) of the voltage applied to the driving electrodes.

5.3.3 THE DIEES CAPACITOR AS SINGLE E-FIELD SENSOR

The work on these new capacitors has carried on with the investigation of the behavior the single ferroelectric capacitor as E-field sensor. Figure 4-46 reports a schematic of the configuration employed with the ferroelectric capacitor connected to the ST conditioning circuit and the charge collector linked to the sensing electrode.

The capacitor C3 – 235-150-50 (red cap) has been used to perform experiments. These capacitor has a bottom electrode of 1010µm, a top electrode of 720µm and a central sensing electrode of 150µm.

Experiments have been performed with an experimental setup almost similar to that discussed in section 5.1.6 and shown in Figure 4-21. A portable version of the setup consisting in two sheet electrodes of 50cm x 50cm and a guard chamber to shield the sensor in order to avoid a direct (i.e., bypassing the charge collector) polarization of the ferroelectric was built. The two electrodes, separated by 10cm, are used to generate a uniform electric field (distance between electrodes can be regulated as you need). Pictures of the setup are given in Figure 4-47.

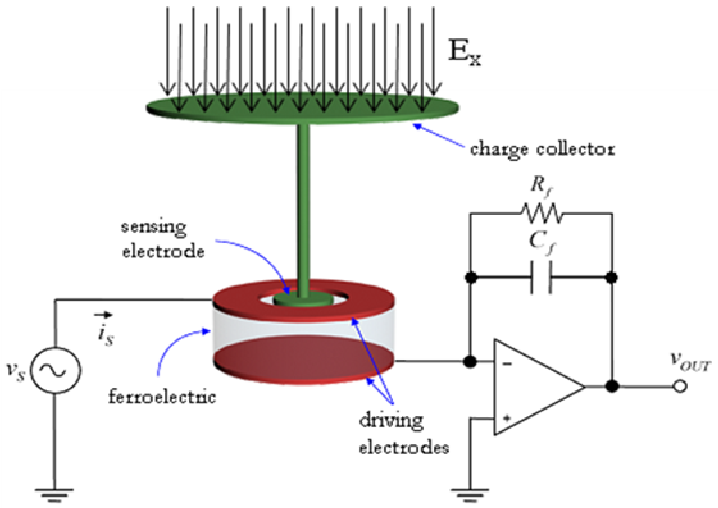

FIGURE 4-46 Schematization of the sensor and the conditioning electronics. CFE and C_f (1.2nF) represent the ferroelectric capacitor and the feedback capacitor respectively, while R_f (2.7MΩ) is used to avoid the drift in the circuit output.

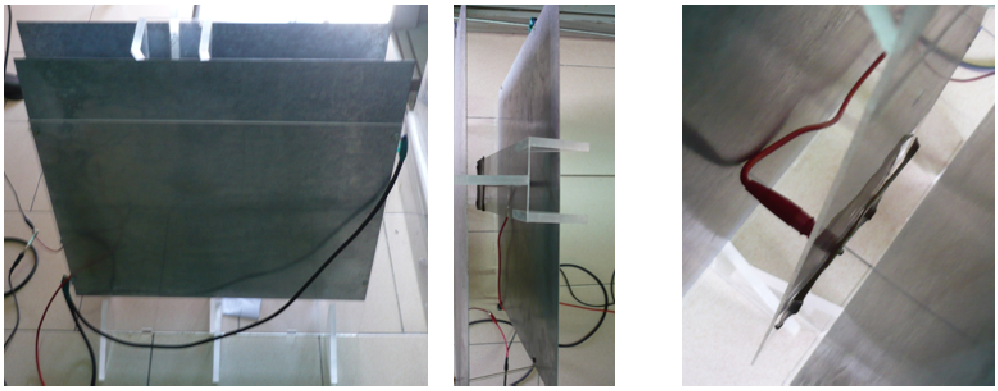

FIGURE 4-47 The setup used to generate the target E-field and the charge collector. Two sheet electrodes of 50cm x 50cm separated by 10cm, are used to generate a uniform electric field (distance between electrodes can be regulated as you need). Three charge collectors, CC1, CC2 and CC3 having dimensions 9cm x 9cm (the one shown in the picture), 20,5cm x 16cm and 25,5cm x 25,5cm have been used to collect the charges induced by the E-field.

An AC voltage is applied to these parallel plates producing the target electric field which, in turn, produces a perturbation of the polarization of the ferroelectric capacitor. The experiments involve subjecting the capacitor to a target E-field having different intensities and frequencies, while also varying the dimensions of the charge collector. Specifically, the voltage (producing the target E-field across the capacitor) applied to the electrodes has been varied in amplitude from $100mV_{pp}$ to $20V_{pp}$ and its frequency varied from 10Hz to 500Hz. Treating the two large electrodes as a parallel plate capacitor, the target electric field amplitudes were 1V/m, 5V/m, 10V/m, 50V/m, 100V/m and 200V/m.
The driving voltage, applied directly to the capacitor plates, has been fixed to $6V_{pp}$@1kHz. All the experiments have been repeated with three charge collectors, CC1, CC2 and CC3 having dimensions 25,5cm x 25,5cm, 20,5cm x 16cm and 9cm x 9cm, respectively.
Figure 4-48 shows examples of the ST output voltage signal obtained by a driving signal of $6V_{pp}$ @ 1kHz and a target electric field of 200 V/m @ 100 Hz and 100 V/m @ 100 Hz.

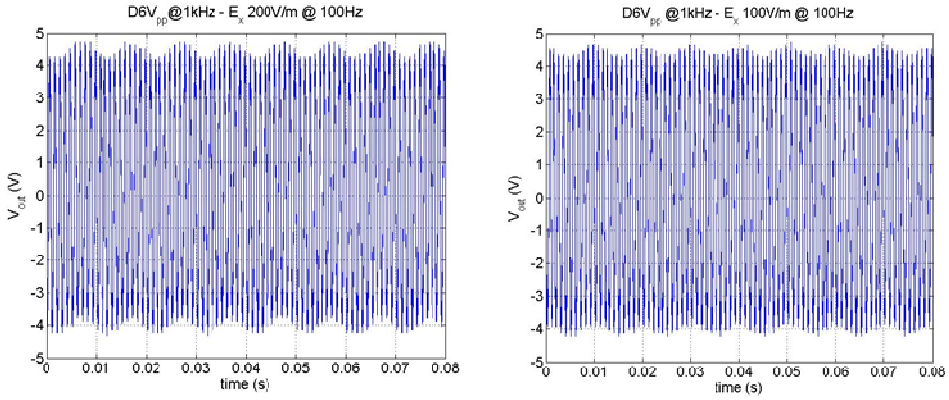

FIGURE 4-48 Examples of experimental ST output voltages signal obtained by a driving signal of 6Vpp @ 1kHz and a target electric field of 200 V/m @ 100 Hz and 100 V/m @ 100 Hz. The effect of the target E-field is clearly visible.

The cases with the higher electric fields has been shown because a more clear effect of the target field on the polarization of the ferroelectric is visible.

Data acquisitions have been also performed with target E-field at 10kHz only to compare the observed effect of an higher frequency (respect to the driving voltage) electric field to the effect of a lower frequency (respect to the driving voltage) electric field on the polarization of the ferroelectric. These data, however, will not be taken in account in the next data investigations. Figure 4-49 shows two examples of hysteresis in the P-E domain obtained by using a driving voltage of $6V_{pp}$@1kHz and perturbing the polarization by sensing electrode with an external E-field of 200V/m at the frequency of 100 Hz and 10 kHz, respectively. The difference in the effect of the external E-field on the polarization in the ferroelectric is clearly visible: an E-field with a frequency lower than the driving signal produces a shift of the hysteresis along the polarization-axes (Figure 4-49a) while a higher frequency E-field produces a clear deformation of the hysteresis (Figure 4-49b). Anyway investigation of the characterization of the capacitor as E-field sensor has been performed by perturbing the ferroelectric by an electric field with a frequency lower than the driving voltage.

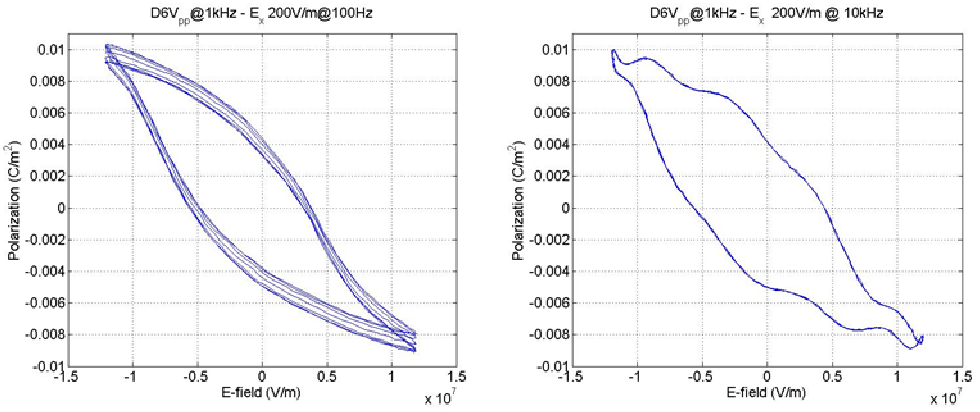

(a) (b)

FIGURE 4-49 Two examples of hysteresis in the P-E domain obtained by using a driving voltage of 6Vpp@1kHz and perturbing the polarization by sensing electrode with an external E-field of 200V/m at the frequency of 100 Hz (a) and 10 kHz (b), respectively. The difference in the effect of the E-field on the polarization is clearly visible.

For an in depth understanding of the effect of the target E-field on the device polarization a spectral analysis of the ST output voltage signals (correlated to the device polarization) has been carried out.

To start, Figure 4-50 shows the comparison of the power spectral density (PSD) in the range (0 -1.2 kHz) of the ST output voltage when no external target E-field is present in both the cases without and with the charge collector linked to the sensing electrode. A peak in the PSD at the frequency of 50Hz appears when the charge collector is linked to the sensing electrode (see the zoom in the Figure 4-50b) due to the electromagnetic fields in the environment. This attests the benefit of the charge collector strategy.

Figures 4-51 shows examples of the power spectral density (PSD) in the range (0 - 1.2kHz) of the ST output voltage signal for four amplitudes of the target electric field (10V/m, 50V/m, 100V/m and 200V/m) at 100Hz, maintaining a driving voltage of $6V_{pp}$@ 1kHz. It is easy to detect the main peak at the frequency (1 kHz) of the driving signal and a smaller one at the frequency of the target field (100Hz). It is clear that a

stronger target signal enhances the height of the peaks at 100Hz in the PSD.

Considering the values of the peaks of the PSD (after conversion from dB/Hz to $V/\sqrt{Hz}$) of the experimental ST output voltages with three charge collectors, the results shown in Figure 4-52 have been obtained for target electric fields with frequencies of 10 Hz (Figure 4-52a) and 100 Hz (Figure 4-52b). A linear interpolation of the experimental observations leads to the parameters (α, β) reported in Table 4-8. A clear dependence of the sensitivity of the device on the dimensions of the charge collector is easy to gather from Figure 4-52.

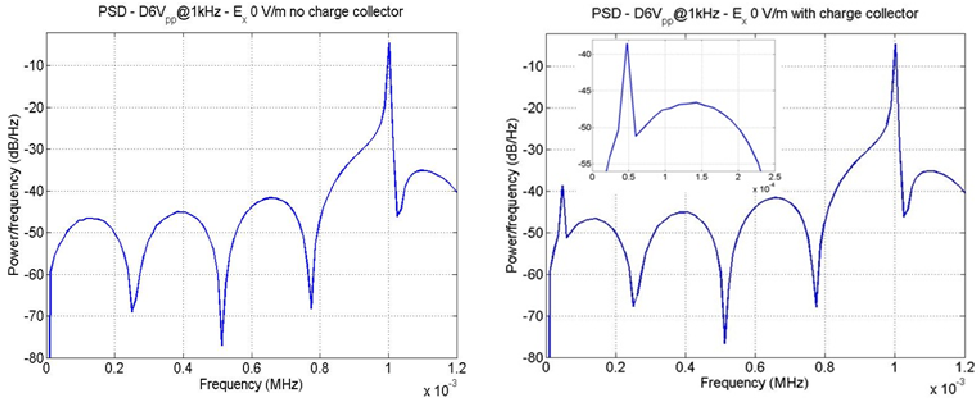

(a) (b)

FIGURE 4-50 The power spectral density (PSD) in the range (0 -1.2 kHz) of the ST output voltage when no external target E-field is present (E_x = 0V/m) in both the cases without (a) and with (b) the charge collector linked to the sensing electrode. In the latter case a peak in the PSD (see zoom in (b)) appears at 50Hz due to the electromagnetic smog in the environment.

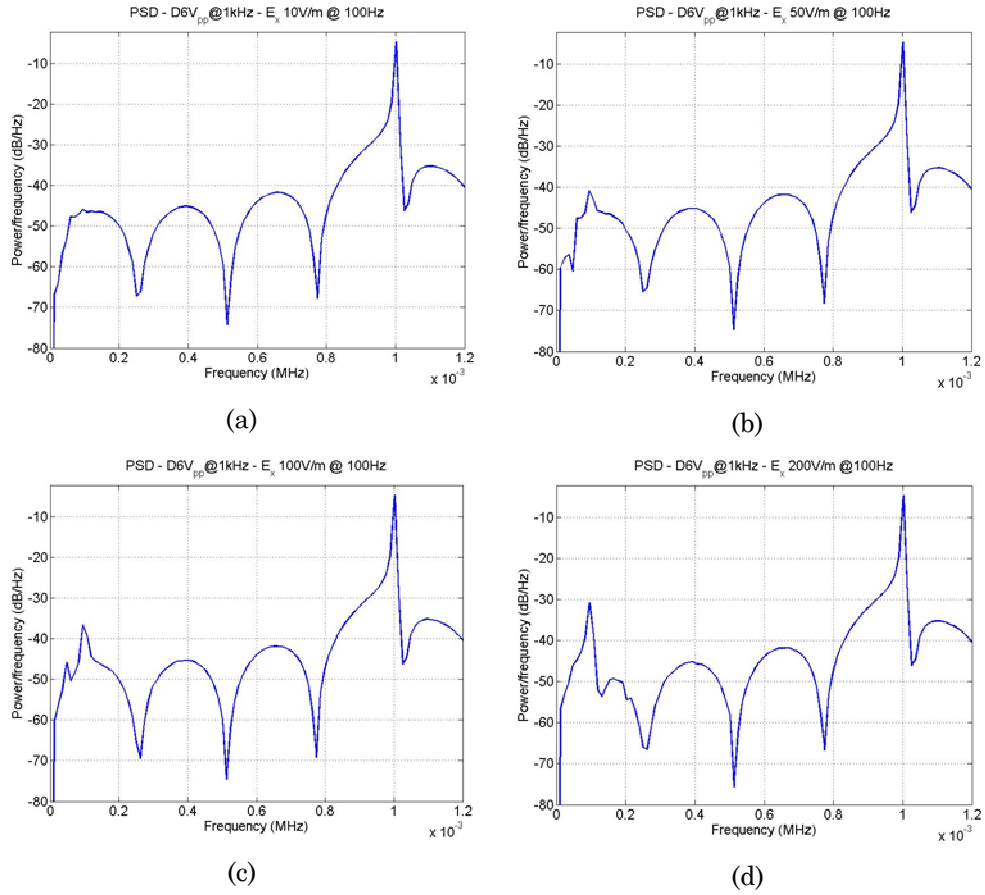

FIGURE 4-51 Examples of the PSD in the range (0 - 1.2kHz) of the ST output voltage signal for four amplitudes of the target electric field: (a) 10V/m, (b) 50V/m, (c) 100V/m and (d) 200V/m, at 100Hz, having fixed a driving voltage of 6Vpp @ 1kHz. A stronger target signal enhances the height of the peaks at 100Hz in the PSD.

Moreover from parameters α in Table 4-8 a dependence on the frequency of the target E-field can be observed. Higher sensitivity have been obtained with a frequency of the target electric field of 10Hz. In general it seems that increasing the frequency of the E-field (then of the field-mill) produces a decreasing of the sensitivity. As a consequence of this result the operative range of the device can be modified by a proper tuning of the device. By a suitable choice of the frequency of the field fill

and of the dimension of the charge collector the operative range can be expanded or restricted.

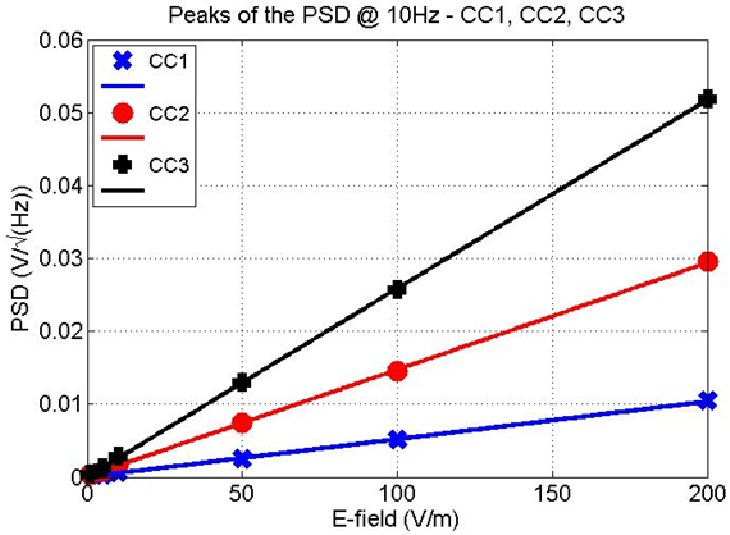

(a)

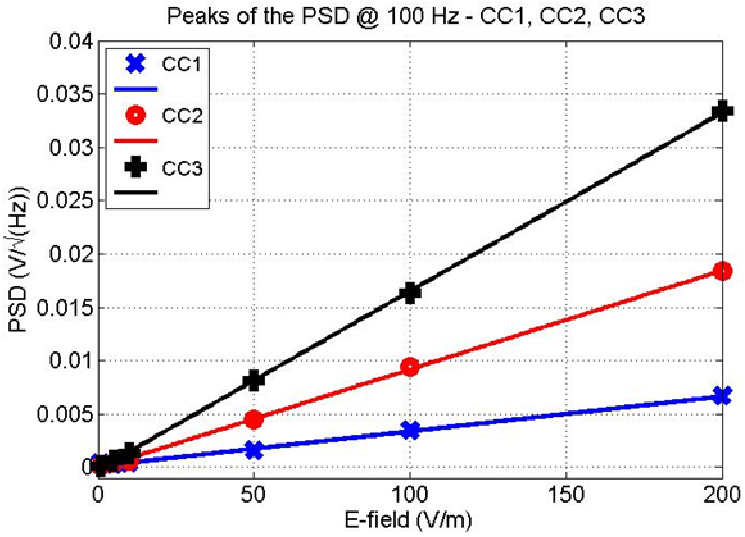

(b)

FIGURE 4-52 Comparison of the peaks of the PSD (V/Hz) of the ST output voltage for target electric fields @10Hz (a) and 100Hz (b) for the three charge collectors CC1, CC2 and CC3.